Cell

Patterning Axon Targeting of Olfactory Receptor Neurons by Coupled Hedgehog Signaling at Two Distinct Steps

Ya-Hui Chou,[1,2] Xiaoyan Zheng,[1,3] Philip A. Beachy,[1,3] and Liqun Luo[1,2,*]
[1]Howard Hughes Medical Institute
[2]Department of Biology
[3]Department of Developmental Biology, School of Medicine
Stanford University, Stanford, CA 94305, USA
*Correspondence: lluo@stanford.edu
DOI 10.1016/j.cell.2010.08.015

SUMMARY

We present evidence for a coupled two-step action of Hedgehog signaling in patterning axon targeting of *Drosophila* olfactory receptor neurons (ORNs). In the first step, differential Hedgehog pathway activity in peripheral sensory organ precursors creates ORN populations with different levels of the Patched receptor. Different Patched levels in ORNs then determine axonal responsiveness to target-derived Hedgehog in the brain: only ORN axons that do not express high levels of Patched are responsive to and require a second step of Hedgehog signaling for target selection. Hedgehog signaling in the imaginal sensory organ precursors thus confers differential ORN responsiveness to Hedgehog-mediated axon targeting in the brain. This mechanism contributes to the spatial coordination of ORN cell bodies in the periphery and their glomerular targets in the brain. Such coupled two-step signaling may be more generally used to coordinate other spatially and temporally segregated developmental events.

INTRODUCTION

From insects to mammals, olfactory receptor neurons (ORNs) expressing a given odorant receptor project their axons to a common glomerulus, thereby creating a spatial map for odor processing (Ressler et al., 1994; Vassar et al., 1994; Mombaerts et al., 1996; Gao et al., 2000; Vosshall et al., 2000). Although ORNs that express a given receptor are distributed widely across the olfactory epithelium, there is a certain degree of spatial correspondence between ORN cell bodies in the periphery and their glomerular targets in the brain. In mice, there is a coarse topographic correspondence of ORNs along the dorsomedial-ventrolateral axis in the nasal epithelium and their glomerular targets along the dorsal-ventral axis of the olfactory bulb (Miyamichi et al., 2005). Axon-axon interactions via Semaphorin-3F and its receptors contribute to the establishment of this topography (Takeuchi et al., 2010). In flies, ORNs belonging to distinct types of sensillae target their axons to different coarse domains in the antennal lobe (Couto et al., 2005). Here, we show that Hedgehog signaling acts via a coupled two-step mechanism to contribute to this spatial coordination in *Drosophila*.

The Hedgehog (Hh) protein acts by binding to and inactivating the Patched (Ptc) receptor, relieving Ptc inhibition of the 7-transmembrane protein Smoothened (Smo). Active Smo transduces the Hh signal to the transcription factor Cubitus interruptus (Ci), which activates transcription of Hh target genes including *ptc* itself (Hooper and Scott, 2005) (Figure 1A). In the *Drosophila* wing disc, Hh is produced and secreted from the posterior compartment, and induces high-level Ptc expression at the anterior-posterior compartment boundary. High Ptc at the boundary in turn sequesters and prevents most of Hh from moving more anteriorly. Meanwhile, in the posterior compartment, the transcription factor Engrailed (En) represses *ci* expression, thus accounting for the lack of Ptc expression in the posterior compartment despite the presence of Hh. The consequence of this Hh signaling loop establishes different Ptc expression levels in different compartments (Hooper and Scott, 2005). The transmembrane proteins Interference hedgehog (Ihog) and Brother of Ihog (Boi) function with Ptc as essential coreceptors involved in binding to and transduction of the Hh signal (Yao et al., 2006; Zheng et al., 2010). In addition to this canonical pathway resulting in the regulation of transcription for developmental patterning, a vertebrate Hedgehog homolog, Sonic Hedgehog (Shh), has also been proposed to act as an axon guidance molecule for spinal commissural neurons (Charron et al., 2003; Bourikas et al., 2005; Okada et al., 2006; Yam et al., 2009). It is unclear whether axon guidance function for Hh signaling is a vertebrate innovation or reflects an evolutionarily conserved function.

During our studies of *Drosophila* olfactory system development, we uncovered a mechanism whereby Hh signaling is used in two distinct but coupled steps. We found that Hh signaling in the larval antennal disc and early pupal antenna creates two populations of ORNs with different Ptc levels. Smo and Ihog are cell-autonomously required in only a subset of ORN classes for their axon targeting. Surprisingly, only

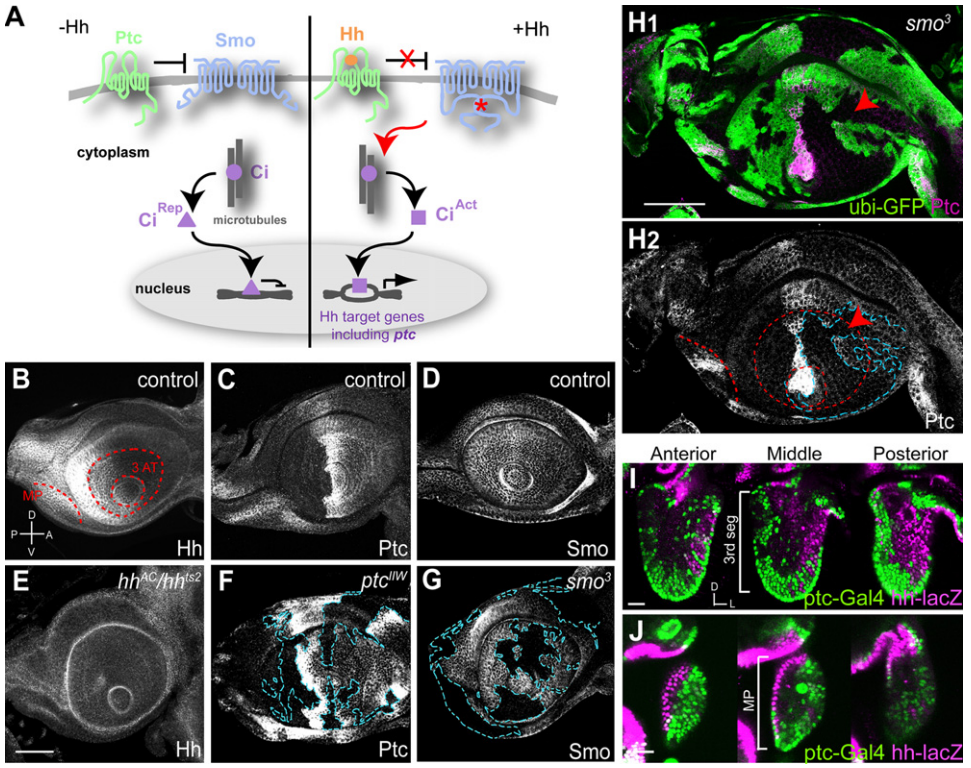

Figure 1. Distribution of Hh, Ptc, and Smo in the Developing Olfactory System

(A) The classic Hh signaling pathway. Left, in the absence of Hedgehog (Hh), Patched (Ptc) inhibits Smoothened (Smo) activity. In the absence of Smo activity, Cubitus interruptus (Ci) is processed to a repressor form (Ci^{Rep}). Right, Hh acts by binding to Ptc and relieving its inhibition of Smo. Active Smo (asterisk) transduces a signal that leads to the maturation of Ci to an activator form (Ci^{Act}). Among genes activated by Ci^{Act} is *ptc* itself.

(B–D) In wild-type control late-third instar larval antennal discs, Hh protein is found in the posterior compartment (B). Ptc protein is highly expressed in the anterior-posterior compartment border, expressed at a medium level in the anterior, and undetectable in the posterior compartment (C). Smo is ubiquitously expressed, with a slightly higher level in the posterior compartment (D).

(E–G) Antennal discs from late-third instar lavae. Hh protein is greatly diminished in hh^{AC}/hh^{ts2} discs from larvae shifted to restrictive temperature 4 hr before dissection (E). Ptc and Smo proteins are greatly diminished in clones homozygous for ptc^{IIW} (F) or smo^{3} (G), respectively. Clone boundaries (blue dashed lines) were determined by loss of the clone marker GFP (see H_1).

(H) Ptc protein is reduced in smo^{3} clones, shown in magenta with green clone marker (H_1) or alone (H_2). Even in the most anterior part of the anterior compartment, there is a reduction of Ptc protein level in smo^{3} clones (arrowheads).

A, anterior; P, posterior; D, dorsal; V, ventral. Red dashed lines in (B) and (H_2) mark the precursor of third segment of antenna (3 AT) and maxillary palp (MP).

(I and J) Cells in the antenna (I) and maxillary palp (J) at 36 hr after puparium formation (APF) labeled by *ptc-Gal4*-driven nuclear GFP (green) and *hh*-nuclear *lacZ* (magenta). Three single confocal sections at anterior, middle and posterior of the right antenna and maxillary palp are shown. Dorsal (D) is up and lateral (L) is right. *Ptc-Gal4* and *hh-lacZ* label complementary populations of cells that are largely spatially segregated, with some intermingling at the border.

The scale bars represent 50 μm (B–H) or 20 μm (I and J). Full genotypes for this and subsequent figures are described in Table S2. Figure S1 provides additional data on Smo, Ptc, Hh, Ihog, and Boi expression in the pupal antenna and maxillary palp, and Smo, Ptc, and Ihog proteins in ORN axons.

low-Ptc ORNs require Smo and Ihog; high-Ptc ORNs do not require Smo and Ihog for their axon targeting. Further genetic analyses, including tissue-specific and temporally regulated loss- and gain-of-function studies of several Hh pathway components, strongly support a coupled two-step model: early Hh signaling in the sensory organ precursors confers differential ORN responsiveness to Hh in the brain, such that only axons of low-Ptc ORN classes respond to later signaling by brain-derived Hh. This coupled two-step mechanism contributes to the spatial coordination of ORN cell bodies in the periphery and their axon targets in the brain, and suggests a general paradigm for coordinating spatially and temporally segregated developmental events.

RESULTS

Hh Signaling Establishes Differential Ptc Protein Levels in ORNs

Drosophila ORNs reside in the third antennal segment and in the maxillary palp (Stocker, 2001). Both structures derive from the larval antennal disc (Figure 1B). We find that Hedgehog (Hh) signaling patterns the larval antennal disc along the anterior-posterior axis. In late third instar larvae, Hh protein is enriched in the posterior compartment of the antennal disc (Figures 1B and 1E), consistent with a previous study based on expression of the *hh-lacZ* enhancer trap (Lee et al., 1992). The level of Ptc protein is highest at the compartment border and moderate in

the anterior compartment (Figures 1C and 1F). Ptc staining in the posterior compartment is indistinguishable from background within clones of cells homozygous for a *ptc* null mutant (Figure 1F), suggesting that the posterior compartment produces either no Ptc or Ptc at a level below the threshold of antibody detection. Smo protein is ubiquitously produced, but higher levels are detected in the posterior compartment (Figures 1D and 1G). In addition, En and Ci proteins are distributed in the posterior and anterior compartments, respectively (data not shown; see Figure 3C), consistent with previous data utilizing *en-lacZ* or *ci* in situ hybridization (Eaton and Kornberg, 1990).

To test whether Hh signaling is necessary for Ptc expression, we generated clones of cells homozygous for a *smo* null mutation (Figure 1G), and found that Ptc expression in the anterior compartment is markedly reduced in *smo* clones (Figure 1H). These expression patterns, together with the *smo* loss-of-function effect on Ptc expression, indicate that antennal disc patterning by the Hh pathway is governed by similar mechanisms as the well-examined wing disc (Hooper and Scott, 2005): cells in the posterior compartment produce Hh and cells in the anterior compartment can respond to Hh. In the wing disc, however, Hh-induced Ptc expression occurs predominantly at the anterior-posterior border (Capdevila et al., 1994; Chen and Struhl, 1996), whereas in the antennal disc, signaling by Hh extends into the entire anterior compartment, as seen by elevated Ptc levels (Figure 1C) that are dependent on Smo (Figure 1H_2, arrowhead). This difference may reflect the fact that the antennal disc is much smaller than the wing disc, thus allowing Hh signaling to occur throughout the anterior compartment including the imaginal precursors of the third antennal segment that give rise to ORNs.

During the first 36 hr after puparium formation (APF), the antennae and maxillary palps undergo extensive morphogenetic movements. ORNs are born and pioneer ORN axons from the antennae and maxillary palps reach the antennal lobe at 18 hr and 32 hr APF, respectively (Jhaveri et al., 2000; Jefferis et al., 2004; Endo et al., 2007; Sweeney et al., 2007). Despite the morphogenetic movements and ORN neurogenesis, the early spatial segregation of cells expressing high levels of Ptc or Hh persists in pupal antennae and maxillary palps (Figures 1I and 1J and Figures S1A and S1B available online), eventually encompassing most ORNs. This is likely a result of continuous Hh signaling between the posterior and anterior compartments during early pupal development (see below). For simplicity, we refer hereafter to these two populations of pupal ORNs as producing high levels of Ptc (high-Ptc) and low levels of Ptc (low-Ptc), although low-Ptc cells may produce no Ptc and high Ptc cells may produce differing amounts of Ptc. Both Ptc and Smo proteins are also present on the ORN axons leaving the antenna as well as the ORN axon layer at the developing antennal lobe (Figures S1C–S1F, S1H, and S1I). These expression studies suggest that Hh signaling is likely involved in ORN development and axon targeting.

Hh Signaling Is Required for Axon Targeting of a Subset of ORN Classes

To examine the requirement for Hh signaling in ORN axon targeting, we performed mosaic analysis (Figure 2A) utilizing a *smo* protein null allele (Figure 1G). First, we used *ey-FLP* to produce homozygous mutant clones in the sensory organs but not in the brain (Newsome et al., 2000; Hummel et al., 2003). We detected mutant clones with the MARCM method (Lee and Luo, 1999), and labeled specific classes of ORNs and their axons with the membrane marker UAS-mCD8GFP coupled to different odorant receptor (OR) promoters driving expression of Gal4 (*Or-Gal4)*. Under these experimental conditions (Figure 2A, top), a large fraction of ORNs are homozygous mutant for *smo*, but Gal4 expression and labeling by mCD8GFP is limited to those mutant ORNs that express the particular *Or-Gal4*. Since Hh is required for proliferation during early development (Cho et al., 2000; Sweeney et al., 2007), a small fraction of mosaic flies have no labeled ORNs due to extreme antennal disc defects. We therefore only analyzed flies with grossly normal antennae and maxillary palps, and brains with ORN axon innervation.

Of the 19 ORN classes examined, nine exhibit notable targeting defects when compared with controls (Table 1, Figure 2B, and Table S1; see also Figure S2 for scoring criteria). In addition to innervating the appropriate glomeruli, *smo* mutant ORN axons mistarget to additional glomeruli or are stalled between glomeruli (arrowheads in Figure 2B and Table S1). The remaining 10 classes exhibit largely normal targeting (Table 1, Figure 2B, and Table S1).

To test whether Smo acts cell autonomously, we made smaller MARCM clones, including single-cell clones, utilizing *hs-FLP* to induce recombination in late third-instar larvae (Figure 2A, bottom). We found targeting defects in 7 of the 9 ORN classes that exhibit defects in *ey-FLP* clones (Table 1, Figure 2B and Table S1). In general there is a lower penetrance of *hs-FLP* induced *smo* phenotypes compared with *ey-FLP*; this likely reflects the perdurance of residual wild-type *smo* mRNA or Smo protein in smaller mutant clones. In addition, we recovered labeled axons in two additional maxillary palp ORNs, and found targeting defects for one, Or46a, but not the other, Or71a. In summary, these genetic mosaic experiments indicate that a subset of ORN classes examined (10/21; bottom rows in Table 1) require Smo, most likely cell autonomously, for axon targeting. Targeting of the remaining 11/21 ORN classes tested does not require Smo.

The class-specific requirement of ORN axon targeting for Smo also extends to Ihog, the coreceptor for Hh (Yao et al., 2006; Zheng et al., 2010). Both Ihog and Boi are expressed in the larval antennal disc, but only Ihog is expressed in pupal ORNs (Figures S1J–S1P). We therefore tested the requirement for Ihog in ORN axon targeting utilizing MARCM analyses (Figure 2A), with a null allele of *ihog* that eliminates Ihog protein (Figure S1K). Unlike *smo* mutant clones, *eyFLP*-induced *ihog* MARCM clones do not create grossly defective antennae and maxillary palps, nor antennal lobes lacking labeled ORN axons. This is likely due to redundancy between Ihog and Boi in larval disc development (Zheng et al., 2010). However, $ihog^{-/-}$ ORN axons exhibit similar targeting defects to those of $smo^{-/-}$ ORN axons (Figure 2B and Table S1). Moreover, the ORN class-specificity of Ihog dependence matches well with that of Smo dependence (Table 1). We further created *hsFLP*-induced small clones in 9 ORN classes that require Smo for axon targeting and observed similar ORN axon mistargeting in most classes, although again at

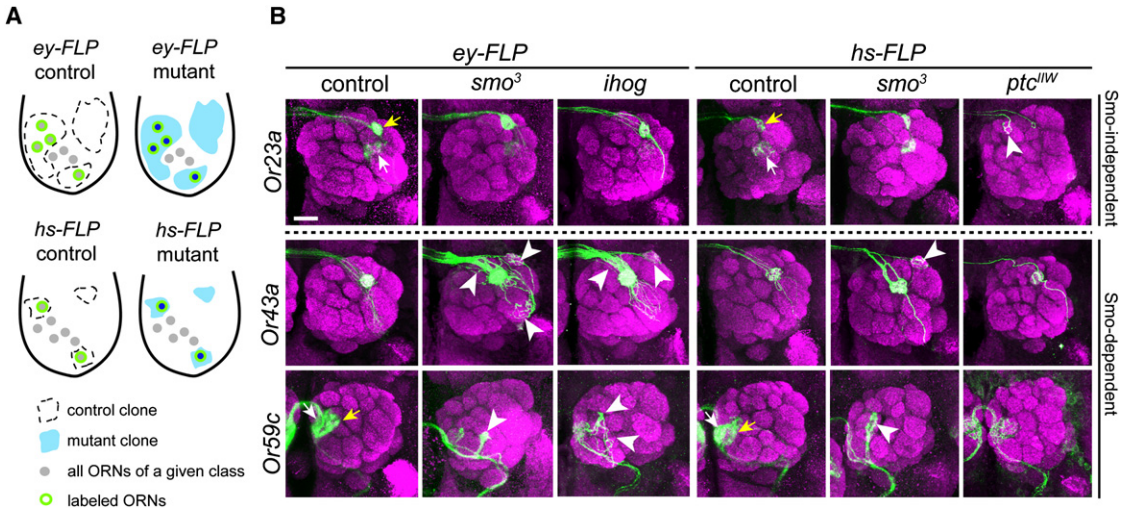

Figure 2. Hh Signaling Is Required for Axon Targeting of a Subset of ORN Classes

(A) Schematic of antennae illustrating mosaic analysis. Cell bodies of a given OR class are shown. *ey-FLP* may create large clones that cover up to 50% of cells in the antennal disc, whereas *hs-FLP* generates small clones. In both cases only ORNs of a given class are labeled because of the use of *Or-Gal4* and MARCM. (B) Examples of ORN axon targeting defects (arrowheads) in *ey-FLP* induced smo^3 and *ihog* clones, and in *hs-FLP* induced smo^3 and ptc^{IIW} clones. Or23a axons target normally in smo^3 and *ihog* mutants but exhibit targeting defects in ptc^{IIW} mutant (arrowhead), whereas Or43a and 59c axons exhibit targeting defects in smo^3 and *ihog* mutants (arrowheads) but normal targeting in ptc^{IIW} mutant clones. Positions of *Or-Gal4* labeled cells remain unchanged in the antenna and maxillary palp in *ey-FLP* induced smo^3 or *ihog* mutant clones (data not shown). Glomeruli are labeled by nc82 (magenta) and ORN axons by *Or-Gal4*-driven mCD8GFP (green). In control, *Or59c-Gal4* is expressed in Or59c ORNs targeting to glomerulus 1 (yellow arrows) and ectopically expressed in ORNs that target to glomerulus VM7 (white arrows). Since VM7 targeting is normal in *smo* mutant as revealed by *Or42a-Gal4* (Table 1), targeting defects in *Or59c-Gal4* labeled ORNs originate from Or59c ORNs. In control, *Or23a-Gal4* is expressed in Or23a ORNs targeting to glomerulus DA3 (yellow arrows) and ectopically expressed in ORNs that target to glomerulus DC3 (white arrows). Since DC3 targeting is normal in *ptc* mutant as revealed by *Or83c-Gal4* (Table 1), targeting defects in *Or23a-Gal4* labeled ORNs originate from Or23a ORNs (see also Figure S2B). The scale bar represents 20 μm.
Table S1 provides more examples of axon targeting in other ORN classes. Figure S2 provides examples to illustrate several criteria for phenotypic scoring.

a lower penetrance likely due to perdurance as in small *smo* clones (Table 1 and Table S1). Together, these results suggest that Hh signaling is cell-autonomously required for axon targeting of only a subset of ORN classes.

Only Low-Ptc ORN Classes Require Hh Signaling for Their Axon Targeting

We have thus far described two observations: (1) Only a subset of ORNs require Smo and Ihog for axon targeting, and (2) Hh signaling in the periphery creates population of cells in the antenna and maxillary palp with different Ptc levels. These observations raise the possibility of a relationship between Ptc levels and Smo-dependence as defined by axon targeting in different ORN classes.

We determined ORN classes that express high and low Ptc using two experiments. First, we used *ptc-Gal4* and *en-Gal4* to label ORNs that are derived from anterior and posterior compartments, respectively (Figures 3A and 3C). We examined their axon projections at 50 hr APF, when stereotypic glomerular structure is first evident. We found that mCD8GFP driven from these two Gal4 lines labels complementary sets of glomeruli (Figures 3A and 3B). Second, based on the correspondence of glomerular identity and OR classes (Couto et al., 2005; Fishilevich and Vosshall, 2005), we double-labeled *hh-lacZ* or *ptc-lacZ* with *Or-Gal4/UAS-mCD8GFP* in late pupal antennae and maxillary palps, and directly confirmed the identity and complementarity of Ptc- and En (Hh)-expressing ORN classes determined by the first experiment (Figure S3). Comparing Ptc levels and Smo-dependence reveals a striking correlation: ORN classes that are not dependent on Smo for axon targeting all belong to the high-Ptc group, whereas all Smo-dependent ORN classes belong to the low-Ptc group (Figure 3B).

In a conventional Hh signaling model, high-Ptc cells are a result of active Hh signaling and should therefore require Smo (Figure 1A). Our finding that high-Ptc classes are not dependent on Smo for ORN axon targeting at first seems counterintuitive. However, we propose a coupled two-step model of Hh signaling based on the presence of Hh in the periphery and brain (see below) to account for these observations (Figure 3C). First, Hh signaling in the sensory organ precursors in the periphery creates ORN groups with different levels of Ptc protein. Then, when encountering a distinct, second source of Hh in the brain, high-Ptc ORN axons are rendered unresponsive by their inability to overcome Ptc inhibition (Taipale et al., 2002; Casali and Struhl, 2004), whereas low-Ptc ORNs are responsive to a new round of Hh signaling and therefore require Smo for axon targeting. Below, we provide further evidence to support this coupled two-step model and rule out other models.

Hh Is Produced by Brain Neurons

The coupled two-step model predicts that ORN axons encounter Hh made in the brain, and that brain-derived Hh is required for

Table 1. Summary of Axon Targeting of 21 ORN Classes in *ey-FLP*- or *hs-FLP*-Induced Control, *smo*, *ihog*, or *ptc* Clones

ORN Class	Glomerular target(s)	*ey-FLP* WT(40A)	*ey-FLP* smo^3	*ey-FLP* *ihog*	*hs-FLP* WT(40A)	*hs-FLP* smo^3	*hs-FLP* *ihog*	*hs-FLP* WT(42D)	*hs-FLP* ptc^{IIW}
Or10a	DL1	8% (24)	8% (26)	6% (16)	not determined (ND)		ND	17% (24)	83% (24)
Or22a	DM2	0% (20)	4% (24)	0% (23)	ND	ND	ND	7% (29)	18% (34)
Or23a	DA3 (DC3)	5% (21)	0% (28)	7% (15)	0% (9)	0% (14)	ND	6% (34)	25% (24)
Or47b	VA1l/m	0% (21)	0% (20)	0% (22)	0% (12)	0% (8)	ND	4% (25)	33% (33)
Or67b	VA3	14% (21)	5% (22)	5% (22)	ND	ND	ND	3% (34)	28% (39)
Gr21a	V	9% (22)	0% (25)	0% (23)	ND	ND	ND	6% (33)	26% (34)
Or42a	VM7 (V, VL2p)	4% (24)	7% (28)	0% (20)	13% (16)	4% (23)	ND	10% (20)	6% (18)
Or47a	DM3	5% (21)	3% (29)	0% (29)	14% (14)	0% (12)	ND	0% (20)	5% (20)
Or71a	VC2	6% (17)	n.i. (39)	0% (22)	8% (12)	0% (26)	ND	7% (28)	6% (31)
Or88a	VA1d	0% (20)	0% (20)	10% (20)	ND	ND	ND	0% (21)	7% (14)
Or92a	VA2	0% (20)	5% (20)	0% (22)	ND	ND	ND	0% (20)	0% (15)
Or9a	VM3	15% (26)	26% (19)	38% (8)	ND	ND	ND	ND	ND
Or13a	DC2	4% (28)	28% (25)	17% (29)	4% (24)	12% (26)	26% (34)	ND	ND
Or43a	DA4l	9% (22)	72% (25)	22% (23)	14% (21)	25% (40)	23% (30)	6% (18)	8% (24)
Or43b	VM2 (DM5)	0% (9)	13% (15)	8% (25)	0% (19)	17% (30)	5% (21)	6% (36)	0% (37)
Or46a	VA7l	10% (20)	n.i. (24)	27% (22)	0% (9)	25% (44)	23% (35)	12% (17)	10% (10)
Or49b	VA5	8% (13)	19% (36)	13% (30)	3% (29)	4% (26)	5% (21)	0% (32)	4% (26)
Or56a	DA2	10% (40)	35% (40)	19% (21)	15% (20)	40% (20)	24% (50)	5% (21)	4% (26)
Or59c	1(VM7)	13% (16)	55% (22)	83% (24)	8% (12)	32% (38)	45% (20)	3% (29)	8% (12)
Or83c	DC3 (VA6)	5% (21)	38% (21)	20% (10)	0% (15)	18% (28)	4% (23)	8% (26)	0% (19)
Or85e	VC1	0% (20)	50% (20)	50% (26)	0% (10)	22% (23)	14% (29)	9% (22)	14% (22)

Percentages represent fraction of brains with targeting defects over total number of brains (in parentheses) that show *Or-Gal4*-driven GFP-positive axons. In the case of *ey-FLP* clones for Or71a and Or46a, none of the brains were innervated by GFP-positive axons (n.i.). The spaced line in the middle divides the ORN classes whose axon targeting do not depend on Smo (above) and those that do (below). Parentheses in the "glomerular target(s)" column indicate the identity of secondary glomeruli targeted by ORNs with ectopic Gal4-expression of particular Or-Gal4 drivers even in controls. These were not counted as phenotypes. All targeting defects were scored blindly to the genotypes. Full genotypes are described in Table S1 and Table S2.

ORN axon targeting. To examine the first question, we performed immunostaining of 24–48 hr APF pupal brains and found that Hh protein is indeed enriched in the antennal lobe peaking at 36 hr APF (Figures S4A–S4D; data not shown), a time when ORN axons make targeting decisions. Hh proteins in the antennal lobe could be contributed by ORNs through axonal transport from the periphery (Huang and Kunes, 1996), or from cells in the brain. To determine the cellular sources for Hh protein at the antennal lobe, we used *UAS-hhRNAi* to knockdown Hh only in the periphery (including all ORNs) or only in the brain. Knocking down Hh in the pupal antenna and maxillary palp but not in the brain using *pebbled (peb)-Gal4* (Sweeney et al., 2007) significantly reduced Hh protein levels in the pupal antenna but not in the antennal lobe (Figures 4A and 4B), consistent with our observation that Hh protein is not detectable in ORN axons leaving the antenna (Figure S1G). Conversely, knocking down Hh in brain neurons but not ORNs using a combination of pan-neural *elav*-Gal4 and *ey*-Gal80 caused a significant reduction of Hh levels in the pupal antennal lobe (Figures 4A and 4B). These results indicate that brain neurons are the main source of Hh protein in the antennal lobe.

To confirm that Hh is expressed in brain neurons, we utilized *hh-Gal4*, an enhancer trap line inserted in the *hh* locus that is expressed identically to *hh-lacZ* in the pupal antenna (data not shown; Tanimoto et al., 2000). *hh-Gal4* labels brain neurons near the antennal lobe, including some olfactory projection neurons (PNs) that send processes into the antennal lobe (Figures S4E and S4F). We further performed MARCM experiments using *hh-Gal4*, and found that *hh-Gal4* is expressed in more neurons than just PNs, and that processes from these neurons cover a large area of the antennal lobe (Figure S4G). Thus, brain-derived Hh in the antennal lobe could influence targeting of ORN axons that possess Smo, Ptc and Ihog proteins (Figure S1).

Brain-Derived Hh Is Required for Axon Targeting of Smo-Dependent ORN Classes

To test the function of brain-derived Hh, we examined ORN axon targeting in animals in which Hh is knocked down in brain neurons but not ORNs. Because of the technical limitation in that we can only visualize ORN axons in a Gal4-independent manner in this experiment, we analyzed 8 ORN classes (4 high-Ptc and 4 low-Ptc) for which we have Or-mCD8GFP or Or-rCD2 transgenes that produce strong axon labeling. We found marked ORN axon targeting defects in four low-Ptc ORN classes, but minimal defects in four high-Ptc classes

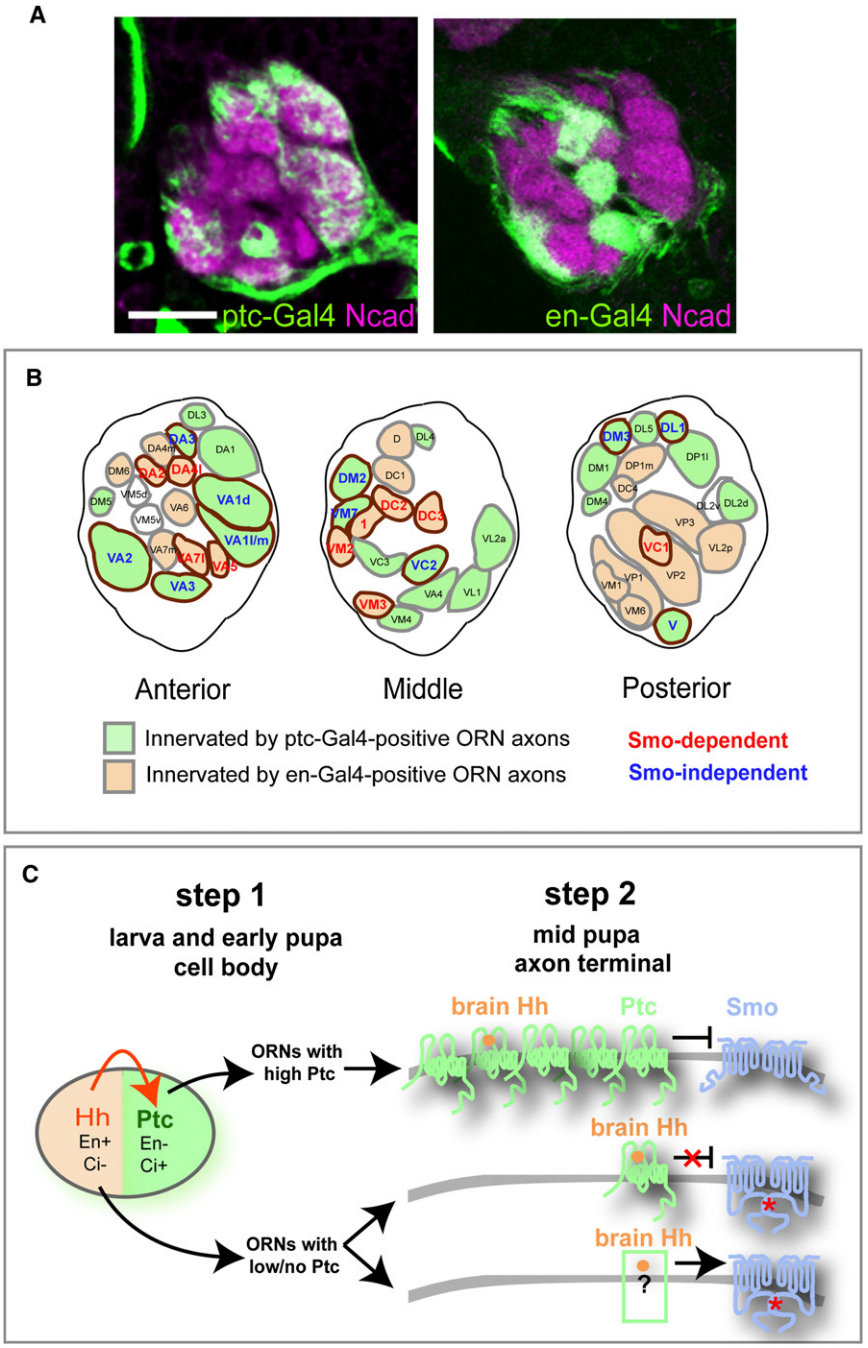

Figure 3. Correlation between Smo Requirement and *ptc* Expression for 21 ORN Classes and a Coupled Two-Step Model

(A) Single confocal sections of antennal lobes at 50 hr APF (stained with N-cadherin in magenta) taken at a similar depth show complementary glomerular innervation of *ptc-Gal4*-positive (left) and *en-Gal4*-positive (right) ORN axons (green). To avoid labeling of glial cells surrounding the antennal lobe with *ptc-Gal4* (data not shown), we used *repo-Gal80* to suppress Gal4 expression in glial cells so that only *ptc-Gal4* positive ORNs are labeled. The scale bar represents 20 μm.

(B) Schematic depiction of the glomerular map in the anterior, middle, and posterior sections of the antennal lobe at 50 hr APF. Glomeruli innervated by *ptc-Gal4* and *en-Gal4* positive ORN axons are filled with green and beige, respectively. Intensities of mCD8GFP vary among *ptc-Gal4*-positive glomeruli, so the assignment is based on the average of GFP expression in nine antennal lobes. One to three antennal lobes have very weak *ptc-Gal4* expression in DA2, DA4m, DA4l, DC3, and VM5v, but are strong for *en-Gal4* (except of VM5v), thus we assign them as *en-Gal4*-positive. Target glomeruli of ORNs whose axon targeting depend on Smo, do not depend on Smo (Table 1), or were not analyzed, are marked by red, blue, or black respectively. Target glomeruli of analyzed ORN classes are circled by brown. Figure S3 provides additional evidence for the correlation of Smo dependence for axon targeting, and *hh*/*ptc* expression in specific ORN classes.

(C) A coupled two-step Hh signaling model for *Drosophila* ORN axon targeting. In step 1, starting from the larval antennal disc and continuing in early pupal antenna and maxillary palp, Hh produced from the posterior compartment (beige) induces Ptc expression in the anterior compartment (green). This results in the generation of two ORN populations with different Ptc levels. The posterior compartment is also marked by the transcription factor Engrailed (En), which promotes *hh* expression and represses *ci* transcription, such that cells in this compartment cannot induce *ptc* expression despite being exposed to Hh. Cells in the anterior compartment lack En and permit *ci* transcription, thereby activating *ptc* expression in response to Hh. In step 2, high-Ptc ORN axons are rendered unresponsive to brain-derived Hh because of an inability to overcome Ptc inhibition; they do not require Smo for axon targeting. ORN axons with low or no Ptc respond to brain-derived Hh, and require Smo for their axon targeting.

(Figures 4C and 4D), suggesting that only low-Ptc ORNs use brain-derived Hh for their axon targeting.

Previous work suggested that ORN axons recognize cues on dendrites of their postsynaptic partner projection neurons (PNs) (Zhu et al., 2006). Brain-derived Hh could in principle influence ORN axon targeting indirectly by specifying the patterning of their postsynaptic partners. Three lines of evidence argue against this possibility. First, MARCM analysis of *smo* or *ptc* mutant PNs did not reveal any mistargeting of PN dendrites (Figure S5). Second, if ORN mistargeting were a consequence of a general perturbation of the target area, there should not be a strong preference for low-Ptc classes to exhibit defects given that glomerular targets of low-Ptc and high-Ptc ORN classes are often nearby (Figure 3B). Third, knocking down brain-derived Hh and removal of Smo or Ihog from ORNs produces similar mistargeting phenotypes (Figure S6A). As a measure of mistargeting

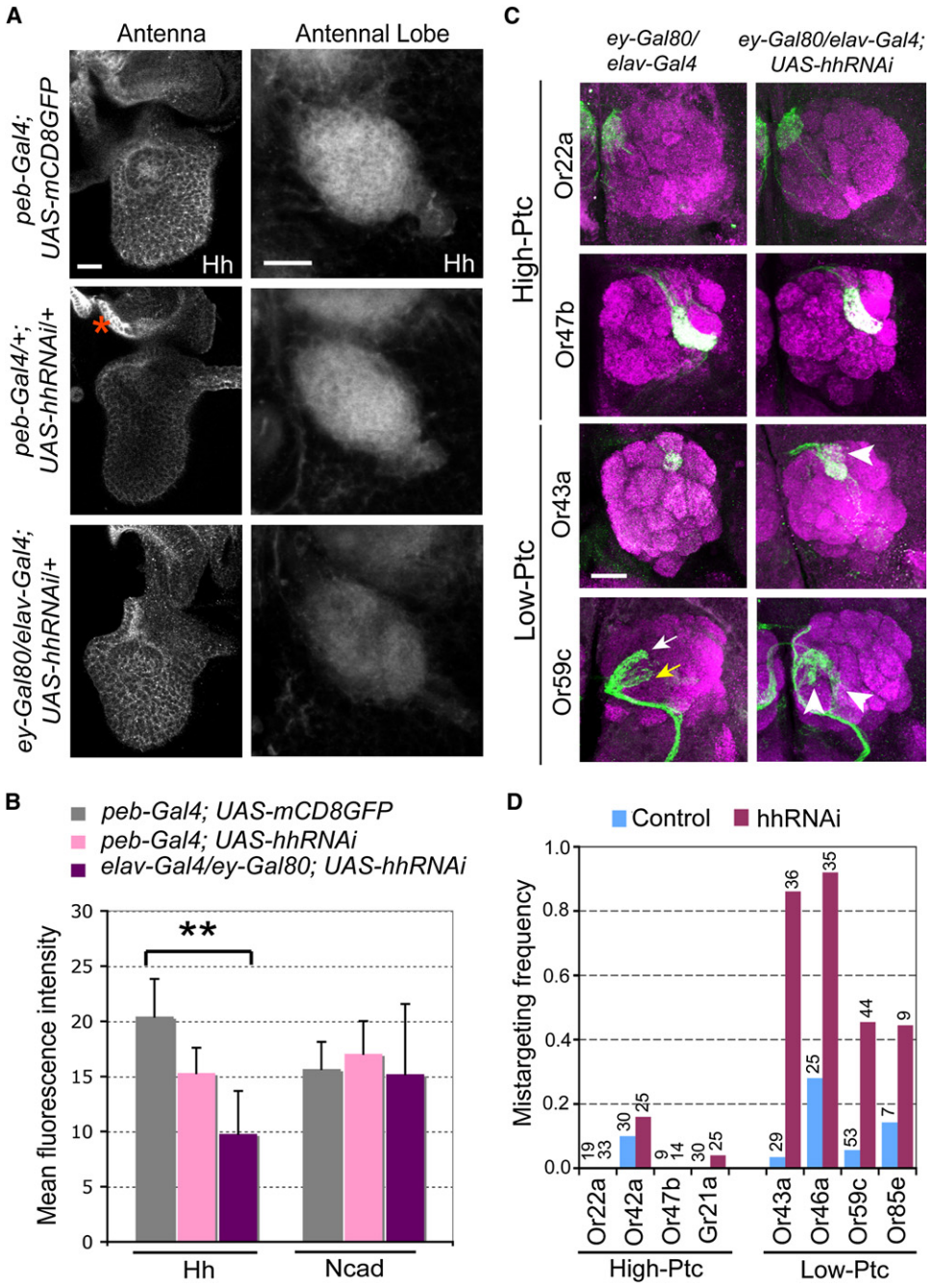

Figure 4. Brain-Derived Hh Is Required for Axon Targeting of Low-Ptc ORN Classes

(A and B) Hh protein levels in antennae and antennal lobes after *RNAi*-mediated Hh knockdown in the periphery or central brain. (A) 36 hr APF pupal antennae (left) and antennal lobes (right) were stained for Hh protein in genotypes of flies labeled on the left. A region lacking *peb-Gal4* expression is marked by an asterisk and serves as control for the knockdown effect of *hhRNAi*. (B) Quantification of relative Hh expression in the antennal lobes. N-cadherin expression in the same antennal lobes was used as control. n = 5–6 for each condition. Data are represented as mean ± SD. **, $p < 0.005$ (unpaired t test). All others: not significantly different from control (*peb-Gal4;UAS-mCD8GFP*).

(C and D) Brain-derived Hh is required for axon targeting of low-Ptc but not high-Ptc ORN classes. (C) Axons of two high-Ptc classes do not exhibit targeting defects (top two rows). Axons of two low-Ptc ORN classes exhibit targeting defects (arrowheads in bottom two rows) when Hh in brain neurons but not ORNs was knocked down during ORN axon targeting. Arrows, normal target glomerulus for Or59c (yellow) and a secondary glomerular target (white). (D) Quantification of axon targeting phenotypes of 8 ORN classes from flies with brain-derived Hh knocked down. Numbers of brains analyzed are shown on top.

Figure S4 provides more data on Hh expression in the pupal brain. Figure S5 provides evidence that Hh signaling is not required for projection neuron dendrite development. Figure S6A provides a comparison of glomerular mistargeting preference of reducing Hh from the brain (Figure 4) and removing Smo or Ihog (Table 1) from ORNs.

preference, we compared phenotypes caused by knockdown of brain-derived Hh and removal of Smo or Ihog in large or small subsets of ORNs by quantifying the glomerular targets of mistargeted axons for the four low-Ptc classes. Despite the different nature of these genetic manipulations (different numbers of ORN axons have disrupted Hh signaling), the mistargeting preferences show more similarity within ORN class using different genetic manipulations (different colors in the same graph in Figure S6A), than within different ORN classes with the same genetic manipulation (the same color across different graphs). Together, these different lines of evidence strongly suggest that brain-derived Hh acts directly on low-Ptc ORN axons to regulate their targeting.

Overexpressing Ptc in Low-Ptc ORN Classes Disrupts Their Axon Targeting

The coupled two-step model predicts that Ptc levels determine the responsiveness of ORN axons to brain-derived Hh. We first tested this prediction by overexpressing Ptc. Compared with controls, *peb-Gal4* driven *UAS-ptc* results in higher Ptc protein levels in most cells in the antenna and in ORN axons at the antennal lobe (Figure 5A). As predicted by our model, this results in ORN axon targeting defects preferentially in low-Ptc classes (Figure 5B, two left columns, and Figure 5C). ORN overexpression of $Ptc^{\Delta loop2}$, which cannot bind Hh but retains its ability to repress Smo (Briscoe et al., 2001), causes similar targeting defects (Figure 5B, middle column, and Figure 5C), suggesting that the essential function of Hh signal is to lift Ptc repression of Smo in low-Ptc ORNs. These defects were also observed when $Ptc^{\Delta loop2}$ was expressed only in low-Ptc cells using *en-Gal4* (Figure 5B, two right columns, and Figure 5C).

Elevating the Ptc level to inhibit Smo activity in low-Ptc classes, therefore, is sufficient to cause targeting defects, consistent with their normal requirement for Smo. The similarity of mistargeting preferences with Ptc overexpression as compared to Smo loss (Figures S6A and S6B) further supports the notion that the effect of Ptc overexpression is caused by inhibiting Smo activity in low-Ptc ORN classes. High-Ptc classes are mostly unaffected (Figure 5B, top row, and Figure 5C), presumably because Smo is already inhibited by endogenous Ptc.

Loss of Ptc in Some High-Ptc ORN Classes Affects Their Axon Targeting by Lifting Smo Inhibition

Next, we examined the consequence of removing endogenous Ptc for ORN axon targeting. We generated small MARCM clones of *ptc* using a null allele (Figure 1F). We found that none of the low-Ptc ORN classes tested require Ptc for axon targeting (Table 1, bottom rows, Figure 2B, Figure S2, and Table S1), consistent with a requirement for pathway activity in these ORNs. Conversely, we found substantial mistargeting for ORN axons lacking Ptc in 6 out of 11 high-Ptc ORN classes (Table 1, top rows, Figure 2B, Figure S2, and Table S1). We do not know why the other five high-Ptc ORN classes behave differently. One possibility is perdurance of Ptc protein in these small clones induced by *hs-FLP.* As Ptc is required for antennal disc patterning, it was difficult to induce large clones with *ey-FLP* without killing the flies or affecting the morphology of antennae and maxillary palps. A second possibility is that the Hh code for axon targeting is not entirely binary (see Discussion). Because Ptc normally inhibits Smo, targeting defects in six high-Ptc ORN classes with Ptc LOF suggest that abnormal activation of Smo in high-Ptc classes causes their axon targeting defects.

It is worth noting that Smo is not required in high-Ptc ORN classes for their axon targeting (Figure 2B and Table 1, top rows). In principle, loss of Smo in the anterior compartment in the first step should result in loss of Ptc expression (Figure 1H), rendering these high-Ptc ORN classes sensitive to brain-derived Hh in the second step. However, since Smo is also required to interpret brain-derived Hh in the second round of signaling, loss of Smo causes these ORN neurons not to respond to brain-derived Hh despite reduced Ptc, therefore remains Smo-independent with regard to axon targeting. Comparison of *smo* and *ptc* clone phenotypes for high-Ptc classes suggests that for proper axon targeting of high-Ptc ORN classes, they should *not* be responsive to brain-derived Hh.

Linking Hh Signaling in the Sensory Organ, Ptc Level, and ORN Axon Targeting

Finally, to test the causal link between Hh expression in the sensory organs, Ptc level and ORN axon targeting, we sought to conditionally inactivate Hh after its function in larval disc patterning is accomplished. We used a temperature-sensitive hh^{ts2} allele, which causes a drastic reduction of Hh protein, and correspondingly reduced Ptc protein levels, within a few hours after shifting to the restrictive temperature (Figure S7A). We employed the *ey-FLP/cell lethal* strategy (Newsome et al., 2000; Hummel et al., 2003) to make the vast majority of cells in the sensory organ homozygous for hh^{ts2}, while leaving the brain heterozygous (Figure 6A). We confirmed a significant reduction of Hh and Ptc protein levels after animals were shifted to the restrictive temperature (Figures S7B–S7E).

When animals were raised at the permissive temperature throughout development, all 6 ORN classes examined exhibit few defects (Figure 6C1). When animals were raised at the restrictive temperature from 2nd instar larva to 45 hr APF (Figure 6C2), axon mistargeting occurs. In addition, a subset of brains lack GFP-labeled axons similar to some cases in *eyFLP*-induced *smo* clones described earlier, reflecting an early function of Hh in antennal disc cell proliferation (Cho et al., 2000; Sweeney et al., 2007). To avoid disrupting this early function, we inactivated Hh by shifting to restrictive temperature between 0–45 hr APF, covering the period of ORN neurogenesis and axon targeting. This largely eliminates the ''no labeled axons'' phenotype while still producing mistargeting phenotypes (Figure 6B). Interestingly, the three high-Ptc classes exhibited much more severe mistargeting phenotypes compared with the three low-Ptc classes (Figure 6C3).

The low axon targeting defects of low-Ptc classes caused by peripheral inactivation of Hh in early pupa support the source of *hh* being derived from the brain. It argues against several alternative models. For example, it is not compatible with peripheral Hh affecting ORN targeting through autocrine or axon-axon interactions among ORNs. If these were the case, one would expect that low-Ptc but not high-Ptc classes be preferentially

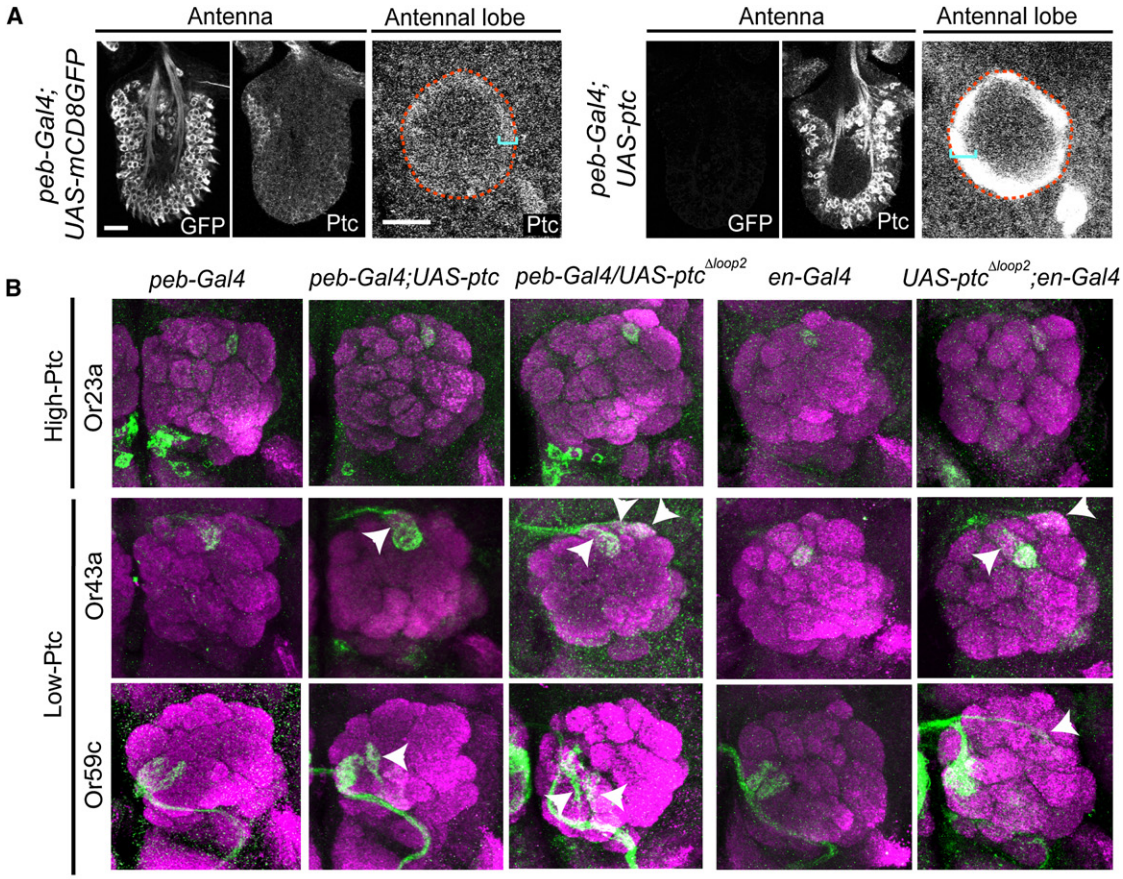

C

ORN Class	Glomerular target(s)	Ptc level	*peb-Gal4*	*peb-Gal4; UAS-ptc*	*peb-Gal4/ UAS-ptc$^{\Delta loop2}$*	*en-Gal4*	*UA Sptc$^{\Delta loop2}$; en-Gal4*
Or22a	DM2	high	6.3% (16)	4% (25)	0% (11)	n.d.	n.d.
Or23a	DA3	high	0% (13)	0% (15)	0% (23)	0% (24)	0% (22)
Or47b	VA1l/m	high	3% (39)	9% (47)	19.2% (26)*	0% (22)	0% (23)
Or67b	VA3	high	0% (17)	7.7% (13)	9.5% (21)*	n.d.	n.d.
Or43a	DA4l	low	0% (11)	75% (20)	69.6% (23)	0% (15)	30% (20)
Or46a	VA7l	low	0% (21)	43.8% (16)	35.5% (31)	0% (18)	29.4% (17)
Or59c	1 (VM7)	low	0% (14)	30.8% (26)	38.9% (18)	0% (24)	13.3% (30)
Or85e	VC1	low	0% (40)	17.4% (23)	28.6% (28)	0% (23)	20% (15)

Figure 5. Overexpressing Ptc Causes Axon Mistargeting of Low-Ptc ORN Classes

(A) The level of Ptc protein is markedly increased in *peb-Gal4*-driven *UAS-ptc* ORNs and the ORN axonal layer in the antennal lobe of 36 hr APF pupae (right panels) as compared to controls (left panels). Antennal lobes are outlined by dashed lines according to N-cadherin staining (data not shown). Brackets denote the ORN axon layer. Control and *peb-Gal4*-driven *UAS-ptc* antennae, maxillary palps, and brains were immunostained in the same tube, distinguished by GFP expression (left images of the antenna panels) and imaged under the same confocal settings.

(B) Overexpressing Ptc and Ptc$^{\Delta loop2}$ in all ORNs by *peb-Gal4*, or overexpressing Ptc$^{\Delta loop2}$ in posterior ORNs by *en-Gal4*, causes targeting defects (arrowheads) in two low-Ptc (Or43a and Or59c) but not in a high-Ptc ORN class (Or23a).

(C) Quantification of ORN axon mistargeting due to Ptc or Ptc$^{\Delta loop2}$ overexpression. * denotes targeting defects that are restricted to near the midline crossing. Figure S6B shows glomerular mistargeting preference for overexpressing Ptc or Ptc$^{\Delta loop2}$ in ORNs.

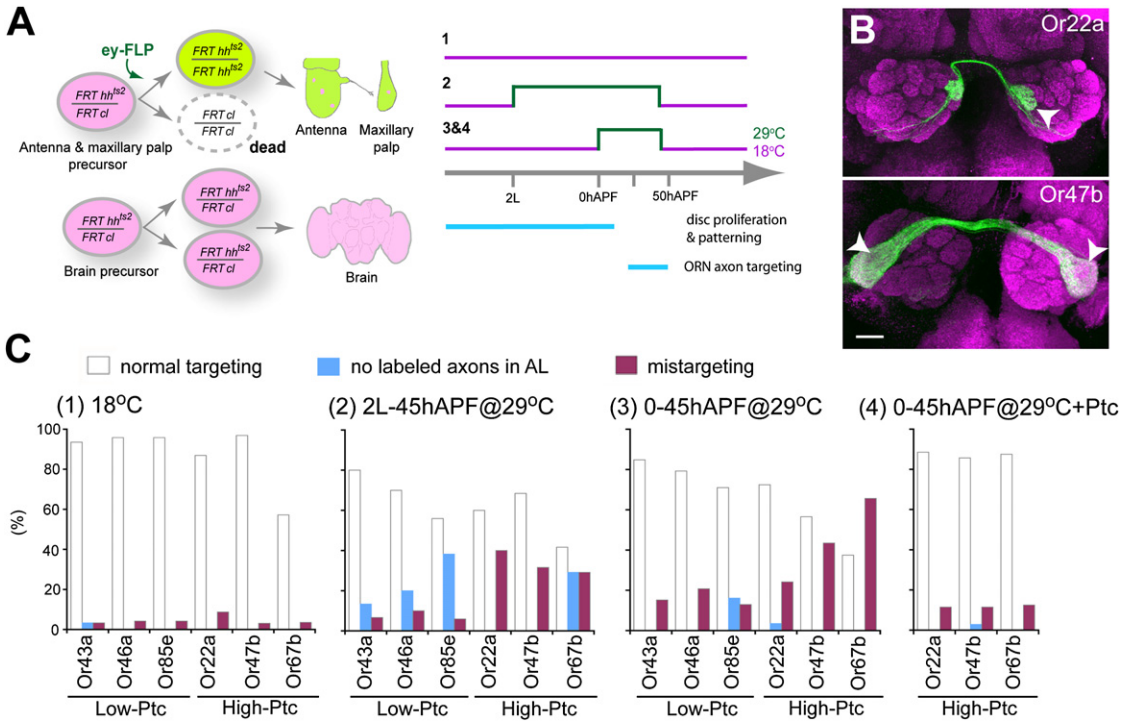

Figure 6. Temporal Inactivation of Peripheral Hh

(A) Schematic of temporally inactivating peripheral Hh with a temperature-sensitive mutation. *ey-FLP* creates hh^{ts2} homozygous clones (green) in antennae and maxillary plaps while other tissues, including the brain, remain heterozygous (magenta). A recessive cell lethal (*cl*) mutation was introduced on the homologous chromosome in trans to hh^{ts2} to eliminate the twinspot of hh^{ts2} homozygous cells (dashed outline). Animals were raised at permissive temperature throughout development except during periods indicated in green when they were shifted to restrictive temperature to inactivate Hh.

(B) Representative images of brains with mistargeted axons (arrowheads) under condition 3. The scale bar represents 20 μm.

(C) Quantification of phenotypes for 6 ORN classes in flies raised at three different temperature paradigms in (A). Condition 4 is identical to condition 3 except that *peb-Gal4* driven *UAS-ptc* is also included.

Figure S7 provides control data for the effectiveness of Hh temporal inactivation.

affected by inactivating peripheral Hh during the period of axon targeting. Two of the three low-Ptc classes (Or46a, Or85e) originate from maxillary palp, whose axon targeting is known to be influenced by axon-axon interactions (Sweeney et al., 2007). Their low targeting defects could be caused by secondary consequence of axon mistargeting of high-Ptc classes through axon-axon interactions.

Why are high-Ptc classes preferentially affected by peripheral inactivation of *hh*? The most likely explanation is that Hh made by early pupal antenna and maxillary palp is used to maintain Ptc expression in high-Ptc ORN classes, which is essential to render their axons insensitive to brain-derived Hh. To test this interpretation, we used *peb-Gal4* to drive *UAS-ptc* to bypass the requirement of Ptc expression by Hh signaling at the early pupal stage. Ptc overexpression alone does not cause mistargeting defect in these high-Ptc classes (Figure 5C). However, it is sufficient to suppress the targeting defects caused by conditional *hh* inactivation in pupal antennae and maxillary palps (Figure 6C4, compared to Figure 6C3).

Together, these results establish a causal link between Hh signaling in the periphery, Ptc level and ORN axon targeting. Hh is required in the antenna and maxillary palp during the early pupal stage to maintain Ptc expression in high-Ptc ORN classes; this then renders high-Ptc ORN axons insensitive to brain-derived Hh when they arrive at the antennal lobe, which is essential for their normal axon targeting.

DISCUSSION

The central finding of this study is the coupled two-step action of Hedgehog in patterning ORN axon targeting (Figure 3C). In the first step, differential Hh pathway activity in peripheral sensory organ precursors in larva and early pupa creates ORN populations with different levels of the Patched receptor. These Patched levels in ORNs then determine axonal responsiveness to target-derived Hh in the brain in the second step: only ORN axons that do not express high levels of Ptc are responsive to and require a second-step of Hh signaling for proper target selection.

Multiple lines of evidence support this model. First, genetic loss-of-function studies indicate that ORNs fall into two groups based on their autonomous requirement for Smo, a classic Hh pathway component, as well as Ihog, a recently discovered positive receptor component for Hh. Second, Smo/Ihog-dependence for axon targeting coincides with Ptc levels for all 21 classes examined (11 high-Ptc and 10 low-Ptc). Third,

knockdown of Hh from brain neurons only affects the targeting of low-Ptc ORN classes, with similar mistargeting preferences as compared to loss of Smo or Ihog in ORNs. Fourth, overexpression of Ptc in ORNs preferentially affects targeting of low-Ptc classes, whereas loss of Ptc in ORNs only affects targeting of high-Ptc classes. Fifth and perhaps most telling, loss of Hh in the antenna and maxillary palp preferentially affects targeting of high-Ptc classes; these mistargeting defects can be suppressed by Ptc overexpression. This result supports two important predictions of the model: Hh from the periphery is not directly required for axon targeting, at least for low-Ptc classes, but is required for the initiation and maintenance of high levels of Ptc in high-Ptc classes. Removing Hh from the periphery results in loss of Ptc expression in high-Ptc ORNs, which lifts Smo inhibition and causes axon mistargeting similar to loss of Ptc. Brain-derived Hh, by contrast, is required for low-Ptc classes but should not be read by at least six high-Ptc classes.

Vertebrate Sonic hedgehog has been proposed to act locally as an axon guidance cue whose action is dependent on the classic Hh pathway component Smo and Boc, an Ihog homolog (Charron et al., 2003; Okada et al., 2006). Our finding that *Drosophila* Hh also plays a role in ORN axon targeting that is dependent on Smo and Ihog suggests an evolutionarily conserved function of Hh in regulating axon development. A recent in vitro study supports the idea that Shh acts directly as an axon guidance cue in a rapid, transcription-independent manner (Yam et al., 2009). In the fly olfactory system, low-Ptc ORN classes originate from the En- and Hh-producing compartment, which are exposed to their own Hh yet do not show a transcriptional response (Figure 3C and data not shown). This is likely because *ci* expression is repressed by En (Eaton and Kornberg, 1990; Schwartz et al., 1995). Brain-derived Hh may thus also act locally in axon targeting, as reported in vitro for Shh (Yam et al., 2009).

Our data do not distinguish whether Hh acts instructively as an axon guidance cue, or permissively to modulate activities of other axon guidance receptors. The primary argument against an instructive model is the lack of spatial patterns of Hh proteins in the antennal lobe (Figure S4D) to account for the spatial distribution of glomerular targets of low- and high-Ptc ORN classes. This does not rule out the instructive model, however, as Hh activity can be modulated post-translationally (Han et al., 2004; Eugster et al., 2007) such that the spatial distribution of Hh activity may differ from Hh protein levels. Alternatively, a permissive model for Hh action on ORN axons is also possible. For instance, Hh may regulate the cAMP/PKA pathway (Jiang and Struhl, 1995; Lepage et al., 1995; Pan and Rubin, 1995; Ogden et al., 2008), which can in turn modulate axon guidance signaling (Song and Poo, 2001). Indeed, it has recently been shown that Shh can modulate axon responsiveness to Semaphorins at the midline of the vertebrate spinal cord (Parra and Zou, 2009).

Whatever the downstream effector, the coupled two-step mechanism uncovered here can be used to coordinate cell body positions of ORNs in the sensory organs and their glomerular targets in the brain. Our data indicate that it is essential both for ORN classes that depend on brain-derived Hh for axon targeting to express low levels of Ptc, and at least a subset of ORN axons that do not respond to brain-derived Hh for axon targeting to express high levels of Ptc, in order to ensure their targeting fidelity. Ptc expression levels thus create a code to diversify ORN classes according to their cell body positions in the sensory organ. Indeed, mistargeting of low-Ptc ORNs in the absence of Smo shows a significant preference for glomeruli that are normally high-Ptc ORN targets (Figure S6C). This switch of axon target is by no means complete, suggesting that Hh signaling works together with other mechanisms to ensure axon targeting fidelity. It has previously been shown that transcription factors Atonal and Amos divide the ORN classes largely according to sensillar groups (Gupta and Rodrigues, 1997; Gupta et al., 1998; Goulding et al., 2000), which might regulate coarse correspondence of ORN cell body positions in periphery and their target glomeruli in the antennal lobe (Couto et al., 2005). The Notch system also diversifies ORN classes within each sensillum (Endo et al., 2007). Our analysis indicates that Hh/Ptc demarcation of ORN cell bodies and their glomerular targets does not coincide precisely with the sensillar groups or with the Notch system (data not shown), suggesting that the Hh system acts to diversify ORN classes independently, and likely at a step in between large sensillar group specification by Atonal/Amos and finer level diversification within each sensillum by the Notch system.

Hh was previously shown to coordinate the development of sensory neurons and their targets in the *Drosophila* visual system: Hh made in photoreceptors is transported down their axons to trigger neurogenesis of target laminar neurons (Huang and Kunes, 1996). The olfactory system is constructed differently: target PNs are born and create a spatial pattern with their dendrites before ORN axon arrival (Jefferis et al., 2001, 2004). Consistent with this idea, Hh signaling is not required for PN development (Figure S5). Despite this fundamental difference from the visual system, Hh signaling is also used, but in a novel manner, to coordinate the ORN cell body position in the sensory organ with the glomerular map in the brain. Hh signaling in the periphery creates populations of ORNs with different Ptc levels such that cells that respond to the Hh signal in the first round are incapable of responding in the second round. Such a coupled two-step mechanism may be generally used for a single signaling pathway to coordinate spatially and/or temporally separate developmental events. Signal-induced expression of a positive or negative pathway component during an early phase of signaling could serve as a time-delayed cellular memory to specify responses at a later stage by rendering cells sensitive or insensitive to a second round of signaling.

EXPERIMENTAL PROCEDURES

Hh Manipulations

hh^{AC}/hh^{ts2} (Figure 1E, and Figure S4B, and Figure S7A) and *FRT82B* hh^{ts2}/*FRT82B ci* (Figure 6 and Figures S7B and S7C) crosses were raised at the permissive temperature (18°C) and shifted to the restricted temperature (29°C) at specific developmental stages as described in the figure legends. The development times (hr) at various temperatures were adjusted to 25°C equivalent. For *peb-Gal4*-driven *UAS-hhRNAi* (Figure 4A), flies were raised at 29°C to maximize Gal4-induced transgene expression.

To knock down brain-derived Hh only (Figures 4A and 4C), we used the pan-neural *elav-Gal4* to knock down Hh expression in all neurons in the brain, but

permitted Hh expression in ORNs by including an additional *ey-Gal80* transgene (Chotard et al., 2005) to inhibit Gal4 activity in ORNs. *tub-Gal80^{ts}* was included to repress Gal4 expression at early and late developmental stages to avoid lethality: crosses were initially raised at 18°C for Gal80^{ts} to suppress Gal4-induced *hhRNAi* expression, followed by shifting to 29°C from early third instar larval stage to 45 hr APF to inactivate Gal80^{ts} and allow *hhRNAi* expression. They were then shifted back to 18°C until eclosion. *elav-Gal4* control flies were raised under the same conditions as *elav-Gal4*-driven *UAS-hhRNAi* flies.

Heatshock induction of MARCM clones labeled by *hh-Gal4* were carried out at 6–9 hr after larval hatching, after extensive search for a time window that allow us to label brain neurons but avoid labeling of *hhGal4*-expressing ORNs (which project strongly labeled axons into the antennal lobe at 36 hr APF, see Figure S4E).

Smo/Ihog/Ptc Manipulations

We used *ey-FLP* to induce MARCM clones of *smo^{3}* and *ihog* only in the antennae and maxillary palps but not in the central brain. *ey-FLP* is expressed throughout disc proliferation, allowing nearly 50% of ORNs to be made homozygous for a normal chromosomal arm (Newsome et al., 2000; Hummel et al., 2003; Komiyama et al., 2004; Zhu and Luo, 2004; Sweeney et al., 2007). However, because *smo* is also required for disc cell proliferation (Sweeney et al., 2007), the total number of *smo* mutant ORNs is likely much less than 50%. *hs-FLP* was used to induce small ORN MARCM clones mutant for *smo^{3}*, *ihog* or *ptc^{IIW}*, and heatshock was performed at late third instar larval stage for 20 min or 1 hr. For *peb-Gal4* and *en-Gal4* driven *UAS-ptc* and *UAS-ptc$^{\Delta loop2}$* experiments (Figure 5), flies were raised at 29°C to increase Gal4-induced transgene expression.

Analysis of Mistargeting Phenotypes and Specificity

All mistargeting phenotypes shown in Table 1 and Figure 6C were scored blindly to genotypes from confocal stacks (see Figure S2). Mistargeted glomeruli of *eyFLP-* and *hsFLP*-induced *smo^{3}* mutants, *elav-Gal4*-driven *hhRNAi*, *eyFLP*-induced *ihog* mutants (Figure S6A), *peb-Gal4*-driven *ptc and ptc$^{\Delta loop2}$* and *en-Gal4*-driven *ptc$^{\Delta loop2}$* (Figure S6B) were analyzed as follows. Each mistageted glomerulus in a given brain was scored as a mistargeting event. The mistargeting frequency of a given glomerulus is equal to (mistargeting events to the glomerulus)/(total brains with mistargeting). The frequency of targeting to glomeruli that are normally targets for high-Ptc ORNs (high-Ptc glomerui; Figure S6C) for a given ORN class is equal to (mistargeting events to all high-Ptc glomeruli)/(total mistargeting events). Mistargeting outside the antennal lobe was excluded from the analysis in Figure S6C.

SUPPLEMENTAL INFORMATION

Supplemental Information includes Extended Experimental Procedures, seven figures, and two tables and can be found with this article online at doi:10.1016/j.cell.2010.08.015.

ACKNOWLEDGMENTS

We thank T. Clandinin, M. Scott, K. Shen, G. Struhl, and members of the Luo lab, in particular L. Sweeney, M. Spletter, D. Berdnik, K. Miyamichi, and T. Mosca for discussion and comments on the manuscript. We are grateful to D. Luginbuhl and S. Wheaton for assistance. We thank T. Tabata, I. Salecker, C.T. Chien, G. Struhl, Y.H. Sun, T. Lee, B. Dickson, R. Holmgren, N.E. Baker, J. Jiang, M.P. Scott, P. Thérond, I. Guerrero, E. Sanchez-Herrero, R. Carthew, G.W. Davis, L.A. Raftery, K. Saigo, Bloomington Stock Center, Kyoto Stock Center, GETDB (NIG), and Developmental Studies Hybridoma Bank for reagents. Supported by an NIH grant (R01-DC005982 to L.L.). L.L. and P.A.B. are HHMI investigators.

Received: December 9, 2009
Revised: May 23, 2010
Accepted: July 26, 2010
Published: September 16, 2010

REFERENCES

Bourikas, D., Pekarik, V., Baeriswyl, T., Grunditz, A., Sadhu, R., Nardo, M., and Stoeckli, E.T. (2005). Sonic hedgehog guides commissural axons along the longitudinal axis of the spinal cord. Nat. Neurosci. *8*, 297–304.

Briscoe, J., Chen, Y., Jessell, T.M., and Struhl, G. (2001). A hedgehog-insensitive form of patched provides evidence for direct long-range morphogen activity of sonic hedgehog in the neural tube. Mol. Cell *7*, 1279–1291.

Capdevila, J., Estrada, M.P., Sanchez-Herrero, E., and Guerrero, I. (1994). The Drosophila segment polarity gene patched interacts with decapentaplegic in wing development. EMBO J. *13*, 71–82.

Casali, A., and Struhl, G. (2004). Reading the Hedgehog morphogen gradient by measuring the ratio of bound to unbound Patched protein. Nature *431*, 76–80.

Charron, F., Stein, E., Jeong, J., McMahon, A.P., and Tessier-Lavigne, M. (2003). The morphogen sonic hedgehog is an axonal chemoattractant that collaborates with netrin-1 in midline axon guidance. Cell *113*, 11–23.

Chen, Y., and Struhl, G. (1996). Dual roles for patched in sequestering and transducing Hedgehog. Cell *87*, 553–563.

Cho, K.O., Chern, J., Izaddoost, S., and Choi, K.W. (2000). Novel signaling from the peripodial membrane is essential for eye disc patterning in Drosophila. Cell *103*, 331–342.

Chotard, C., Leung, W., and Salecker, I. (2005). glial cells missing and gcm2 cell autonomously regulate both glial and neuronal development in the visual system of Drosophila. Neuron *48*, 237–251.

Couto, A., Alenius, M., and Dickson, B.J. (2005). Molecular, anatomical, and functional organization of the Drosophila olfactory system. Curr. Biol. *15*, 1535–1547.

Eaton, S., and Kornberg, T.B. (1990). Repression of ci-D in posterior compartments of Drosophila by engrailed. Genes Dev. *4*, 1068–1077.

Endo, K., Aoki, T., Yoda, Y., Kimura, K., and Hama, C. (2007). Notch signal organizes the Drosophila olfactory circuitry by diversifying the sensory neuronal lineages. Nat. Neurosci. *10*, 153–160.

Eugster, C., Panakova, D., Mahmoud, A., and Eaton, S. (2007). Lipoprotein-heparan sulfate interactions in the Hh pathway. Dev. Cell *13*, 57–71.

Fishilevich, E., and Vosshall, L.B. (2005). Genetic and functional subdivision of the Drosophila antennal lobe. Curr. Biol. *15*, 1548–1553.

Gao, Q., Yuan, B., and Chess, A. (2000). Convergent projections of Drosophila olfactory neurons to specific glomeruli in the antennal lobe. Nat. Neurosci. *3*, 780–785.

Goulding, S.E., zur Lage, P., and Jarman, A.P. (2000). amos, a proneural gene for Drosophila olfactory sense organs that is regulated by lozenge. Neuron *25*, 69–78.

Gupta, B.P., Flores, G.V., Banerjee, U., and Rodrigues, V. (1998). Patterning an epidermal field: Drosophila lozenge, a member of the AML-1/Runt family of transcription factors, specifies olfactory sense organ type in a dose-dependent manner. Dev. Biol. *203*, 400–411.

Gupta, B.P., and Rodrigues, V. (1997). Atonal is a proneural gene for a subset of olfactory sense organs in Drosophila. Genes Cells *2*, 225–233.

Han, C., Belenkaya, T.Y., Wang, B., and Lin, X. (2004). Drosophila glypicans control the cell-to-cell movement of Hedgehog by a dynamin-independent process. Development *131*, 601–611.

Hooper, J.E., and Scott, M.P. (2005). Communicating with Hedgehogs. Nat. Rev. Mol. Cell Biol. *6*, 306–317.

Huang, Z., and Kunes, S. (1996). Hedgehog, transmitted along retinal axons, triggers neurogenesis in the developing visual centers of the Drosophila brain. Cell *86*, 411–422.

Hummel, T., Vasconcelos, M.L., Clemens, J.C., Fishilevich, Y., Vosshall, L.B., and Zipursky, S.L. (2003). Axonal targeting of olfactory receptor neurons in Drosophila is controlled by Dscam. Neuron *37*, 221–231.

Jefferis, G.S., Vyas, R.M., Berdnik, D., Ramaekers, A., Stocker, R.F., Tanaka, N.K., Ito, K., and Luo, L. (2004). Developmental origin of wiring specificity in the olfactory system of Drosophila. Development *131*, 117–130.

Jefferis, G.S.X.E., Marin, E.C., Stocker, R.F., and Luo, L. (2001). Target neuron prespecification in the olfactory map of Drosophila. Nature *414*, 204–208.

Jhaveri, D., Sen, A., and Rodrigues, V. (2000). Mechanisms underlying olfactory neuronal connectivity in Drosophila-the atonal lineage organizes the periphery while sensory neurons and glia pattern the olfactory lobe. Dev. Biol. *226*, 73–87.

Jiang, J., and Struhl, G. (1995). Protein kinase A and hedgehog signaling in Drosophila limb development. Cell *80*, 563–572.

Komiyama, T., Carlson, J.R., and Luo, L. (2004). Olfactory receptor neuron axon targeting: intrinsic transcriptional control and hierarchical interactions. Nat. Neurosci. *7*, 819–825.

Lee, J.J., von Kessler, D.P., Parks, S., and Beachy, P.A. (1992). Secretion and localized transcription suggest a role in positional signaling for products of the segmentation gene hedgehog. Cell *71*, 33–50.

Lee, T., and Luo, L. (1999). Mosaic analysis with a repressible cell marker for studies of gene function in neuronal morphogenesis. Neuron *22*, 451–461.

Lepage, T., Cohen, S.M., Diaz-Benjumea, F.J., and Parkhurst, S.M. (1995). Signal transduction by cAMP-dependent protein kinase A in Drosophila limb patterning. Nature *373*, 711–715.

Miyamichi, K., Serizawa, S., Kimura, H.M., and Sakano, H. (2005). Continuous and overlapping expression domains of odorant receptor genes in the olfactory epithelium determine the dorsal/ventral positioning of glomeruli in the olfactory bulb. J. Neurosci. *25*, 3586–3592.

Mombaerts, P., Wang, F., Dulac, C., Chao, S.K., Nemes, A., Mendelsohn, M., Edmondson, J., and Axel, R. (1996). Visualizing an olfactory sensory map. Cell *87*, 675–686.

Newsome, T.P., Asling, B., and Dickson, B.J. (2000). Analysis of Drosophila photoreceptor axon guidance in eye-specific mosaics. Development *127*, 851–860.

Ogden, S.K., Fei, D.L., Schilling, N.S., Ahmed, Y.F., Hwa, J., and Robbins, D.J. (2008). G protein Galphai functions immediately downstream of Smoothened in Hedgehog signalling. Nature *456*, 967–970.

Okada, A., Charron, F., Morin, S., Shin, D.S., Wong, K., Fabre, P.J., Tessier-Lavigne, M., and McConnell, S.K. (2006). Boc is a receptor for sonic hedgehog in the guidance of commissural axons. Nature *444*, 369–373.

Pan, D., and Rubin, G.M. (1995). cAMP-dependent protein kinase and hedgehog act antagonistically in regulating decapentaplegic transcription in Drosophila imaginal discs. Cell *80*, 543–552.

Parra, L.M., and Zou, Y. (2009). Sonic hedgehog induces response of commissural axons to Semaphorin repulsion during midline crossing. Nat. Neurosci. *13*, 29–35.

Ressler, K.J., Sullivan, S.L., and Buck, L.B. (1994). Information coding in the olfactory system: evidence for a stereotyped and highly organized epitope map in the olfactory bulb. Cell *79*, 1245–1255.

Schwartz, C., Locke, J., Nishida, C., and Kornberg, T.B. (1995). Analysis of cubitus interruptus regulation in Drosophila embryos and imaginal disks. Development *121*, 1625–1635.

Song, H., and Poo, M. (2001). The cell biology of neuronal navigation. Nat. Cell Biol. *3*, E81–E88.

Stocker, R.F. (2001). Drosophila as a focus in olfactory research: mapping of olfactory sensilla by fine structure, odor specificity, odorant receptor expression, and central connectivity. Microsc. Res. Tech. *55*, 284–296.

Sweeney, L.B., Couto, A., Chou, Y.H., Berdnik, D., Dickson, B.J., Luo, L., and Komiyama, T. (2007). Temporal target restriction of olfactory receptor neurons by Semaphorin-1a/PlexinA-mediated axon-axon interactions. Neuron *53*, 185–200.

Taipale, J., Cooper, M.K., Maiti, T., and Beachy, P.A. (2002). Patched acts catalytically to suppress the activity of Smoothened. Nature *418*, 892–897.

Takeuchi, H., Inokuchi, K., Aoki, M., Suto, F., Tsuboi, A., Matsuda, I., Suzuki, M., Aiba, A., Serizawa, S., Yoshihara, Y., et al. (2010). Sequential arrival and graded secretion of Sema3F by olfactory neuron axons specify map topography at the bulb. Cell *141*, 1056–1067.

Tanimoto, H., Itoh, S., ten Dijke, P., and Tabata, T. (2000). Hedgehog creates a gradient of DPP activity in Drosophila wing imaginal discs. Mol. Cell *5*, 59–71.

Vassar, R., Chao, S.K., Sitcheran, R., Nunez, J.M., Vosshall, L.B., and Axel, R. (1994). Topographic organization of sensory projections to the olfactory bulb. Cell *79*, 981–991.

Vosshall, L.B., Wong, A.M., and Axel, R. (2000). An olfactory sensory map in the fly brain. Cell *102*, 147–159.

Yam, P.T., Langlois, S.D., Morin, S., and Charron, F. (2009). Sonic hedgehog guides axons through a noncanonical, Src-family-kinase-dependent signaling pathway. Neuron *62*, 349–362.

Yao, S., Lum, L., and Beachy, P. (2006). The ihog cell-surface proteins bind Hedgehog and mediate pathway activation. Cell *125*, 343–357.

Zheng, X., Mann, R.K., Sever, N., and Beachy, P.A. (2010). Genetic and biochemical definition of the Hedgehog receptor. Genes Dev. *24*, 57–71.

Zhu, H., Hummel, T., Clemens, J.C., Berdnik, D., Zipursky, S.L., and Luo, L. (2006). Dendritic patterning by Dscam and synaptic partner matching in the Drosophila antennal lobe. Nat. Neurosci. *9*, 349–355.

Zhu, H., and Luo, L. (2004). Diverse functions of N-cadherin in dendritic and axonal terminal arborization of olfactory projection neurons. Neuron *42*, 63–75.